The Non-Covalently Bound SO···H2O System, Including an Interpretation of the Differences Between SO···H2O and O2···H2O

Journal:	*Physical Chemistry Chemical Physics*
Manuscript ID	CP-ART-09-2018-005749.R2
Article Type:	Paper
Date Submitted by the Author:	05-Nov-2018
Complete List of Authors:	Misiewicz, Jonathon; University of Georgia, Computational Chemistry Noonan, Julia; University of Georgia; Taylor University Turney, Justin; University of Georgia, Center for Computational Chemistry Schaefer, Henry; University of Georgia, Computational Chemistry

Journal Name

ARTICLE TYPE

Cite this: DOI: 10.1039/xxxxxxxxxx

The Non-Covalently Bound $SO\cdots H_2O$ System, Including an Interpretation of the Differences Between $SO\cdots H_2O$ and $O_2\cdots H_2O$†

Jonathon P. Misiewicz,[a] Julia A. Noonan,[ab] Justin M. Turney,[a] and Henry F. Schaefer III[a*]

Received Date
Accepted Date

DOI: 10.1039/xxxxxxxxxx

www.rsc.org/journalname

Despite the interest in sulfur monoxide (SO) among astrochemists, spectroscopists, inorganic chemists, and organic chemists, its interaction with water remains largely unexplored. We report the first high level theoretical geometries for the two minimum energy complexes formed by sulfur monoxide and water, and we report energies using basis sets as large as aug-cc-pV(Q+d)Z and correlation effects through perturbative quadruple excitations. One structure of $SO\cdots H_2O$ is hydrogen bonded and the other chalcogen bonded. The hydrogen bonded complex has an electronic energy of –2.71 kcal mol^{-1} and a zero kelvin enthalpy of –1.71 kcal mol^{-1}, while the chalcogen bonded complex has an electronic energy of –2.64 kcal mol^{-1} and a zero kelvin enthalpy of –2.00 kcal mol^{-1}. We also report the transition state between the two structures, which lies below the $SO\cdots H_2O$ dissociation limit, with an electronic energy of –1.26 kcal mol^{-1} and an enthalpy of –0.81 kcal mol^{-1}. These features are much sharper than for the isovalent complex of O_2 and H_2O, which only possesses one weakly bound minimum, so we further analyze the structures with open-shell SAPT0. We find that the interactions between O_2 and H_2O are uniformly weak, but the $SO\cdots H_2O$ complex surface is governed by the superior polarity and polarizability of SO, as well as the diffuse electron density provided by sulfur's extra valence shell.

* Corresponding Author
[a] *Center for Computational Quantum Chemistry, University of Georgia, Athens, Georgia. E-mail: ccq@uga.edu*
[b] *Taylor University, Upland, Indiana*

† Electronic Supplementary Information (ESI) available: geometries, vibrational frequencies, orbital occupation, SCF energies, multireference diagnostics, IRC trajectories. See DOI: 10.1039/b000000x/

1 Introduction

Sulfur monoxide (SO) is a highly reactive biradical that quickly disproportionates into S_2O and SO_2.[1–3] Despite this, the compound is of interest in several different areas of chemistry. Sulfur compounds are known to be of special importance to the formation of aerosols, the chemistry of which is far from fully understood.[4] Sulfur monoxide is known to be an intermediate in atmospheric sulfur oxidation processes, being formed by oxidation of elemental sulfur[5] and itself being oxidized to form SO_2[6,7] and SO_3.[8] Its importance in sulfur oxidation has also led to it being considered a major intermediate in the combustion of sulfur compounds[9] and included in sulfur combustion mechanisms.[10–12] Sulfur monxoide can undergo additional reactions with dienes to produce unsaturated cyclic sulfoxides,[13–15] and even the excited singlet state can now be transferred.[16] It is a known ligand in inorganic synthesis.[17–24] Its electronic,[25–27] rotational,[28,29], and vibrational[30–34] spectra have all been thoroughly analyzed. Theory correctly predicted, prior to experiment, the assignment of electronic transitions involving emissions from the c $^1\Sigma^-$ and A′ $^1\Delta$ states of SO,[35] as well as the fundamental vibrational frequency of the A″ $^3\Sigma^+$electronic state.[36]

However, sulfur monoxide is probably of greatest interest to astrochemists. The highly reactive SO can be long-lived in the near vacuum of space, so it is present in relatively large abundance.[37] Astrochemists have used its spectroscopic signatures to gauge the lifetimes of stars and to probe magnetic field intensities.[38] SO can be used to determine if a star is in the hot core phase of development, or if a region of space is dominated by shock waves,[39] and it can potentially identify disk winds.[40] There is also evidence of its existence on the Jovian moon Io[41–43] as well as Venus.[44,45]

Despite all this, SO remains so understudied that even its interaction with water remains mysterious. Two studies have considered reactions that form H_2O and SO in the excited $^1\Delta$ state. Montoya, Sendt, and Haynes[46] computed ΔH_{0K} for three possible reactions between water and $^1\Delta$ SO. Frank, Sadílek, Ferrier, and Tureček[47] concluded computationally that water and $^1\Delta$ SO were possible dissociation products of dihydroxysulfane. They performed neutralization-reionization mass spectrometry on dihydroxysulfane and observed SO and H_2O formation with respective rate constants of $4.3 \pm 0.4 \times 10^5$ and 4×10^4 s^{-1}.

Recently, Wakelam, Loison, Mereau, and Ruaud[48] computed geometries and binding energies for

the complex between H_2O and $^3\Sigma^-$ SO to model the desorption of SO from ice surfaces. The theoretical results of reference 48 differ from those reported here in several respects. Wakelam et al. reported three geometries computed at M06-2X/aug-cc-pVTZ. Correspondence with the authors revealed that one was an energy minimum bound with an electronic energy of 3.1 kcal mol^{-1}. The other two SO$\cdots$H$_2$O stationary points were concluded to be transition states with activation energies of 0.6 and 1.1 kcal mol^{-1}, with respect to separated SO plus H_2O.

One might expect this system to be similar to the well-studied $O_2\cdots H_2O$ system, since O_2 and SO are isovalent. However, the $O_2\cdots H_2O$ complex has a dissociation energy of only 0.64 kcal mol^{-1}, and the eleven known first and second order saddle points are all within 0.50 kcal mol^{-1} of the global minimum.[49,50] The surface is so flat that due to nuclear delocalization, the ground state rotational wavefunction is of C_{2v} symmetry, despite a C_s minimum geometry.[49,51] The features of the SO$\cdots$H$_2$O potential surface reported by Wakelam et al. appear much less flat.

To discover why the potential energy surface for the $O_2\cdots H_2O$ complex from experiment and theory is so different from the SO$\cdots$H$_2$O stationary points reported by Wakelam et al., we employ high levels of *ab initio* theory to accurately compute the surface of this important complex and to provide a physical interpretation for the computational results.

2 Theoretical Methods

2.1 Geometries

The geometries of all open-shell species studied were optimized using unrestricted coupled cluster theory with single, double, and perturbative triple excitations [UCCSD(T)] on a restricted open-shell reference (ROHF).[52,53]. The one closed-shell species, water, was studied by the analogous closed-shell methods.[54,55] All geometry optimizations and harmonic vibrational frequencies were computed in MOLPRO 2010.1.[56] For all these computations, the core electrons occupying the 1*s* shell of oxygen atoms and the 1*s*, 2*s*, and 2*p* shells of sulfur atoms were not correlated. The Hartree–Fock densities were converged to within 10^{-11} and the coupled cluster energies were converged to within 10^{-12} Hartree. The internal coordinates of each geometry were converged to a root mean square force of 10^{-8} Hartree Bohr^{-1} using the four-point gradient.

Previous research has demonstrated that the use of different basis sets can change the number of

imaginary modes for a stationary point on the isovalent $O_2\cdots H_2O$ surface.[50] Thus the basis set dependence of the optimal geometry for the $SO\cdots H_2O$ complex reported by Wakelam et al. was investigated before deciding what basis set should be used for the remainder of this study. Initial optimizations were performed with the cc-pV(X+d)Z and aug-cc-pV(X+d)Z families of basis sets, where X = (D, T, Q).[57–60] The potential around the torsional angle between the O of SO and the water molecule was found to be very flat, and for the cc-pV(X+d)Z basis sets, this resulted in changes in the dihedral angle of over 30°, depending on the basis set truncation level. By contrast, the augmented basis sets consistently found the torsional angle of the minimum at 180 degrees, enforcing C_s symmetry at each basis set truncation level. To confirm that the different behavior was due solely to the use of augmented functions, the computations were repeated with the cc-pwCVXZ and aug-cc-pwCVXZ families of basis sets,[61] which provide an alternate treatment of the tight *d* functions needed for third row atoms, such as sulfur. The results were found to be similar to those from the non-core-weighted basis sets, so all further computations were performed with the aug-cc-pV(X+d)Z family of basis sets.

Harmonic vibrational frequencies were then computed using finite differences of energies at the same level of theory as the optimized structures. All reported transition states had a single imaginary frequency, while the other stationary points had all real frequencies. The optimized geometries and vibrational frequencies are reported in the Supplementary Information.†

As our investigation discovered two minimum energy $SO\cdots H_2O$ complexes, we also optimized a transition state connecting the two structures. The connectivity was confirmed by an intrinsic reaction coordinate (IRC) computation using the Gonzalez–Schlegel algorithm[62] in a locally modified version of Psi4,[63] using finite differences of energies. The energies were computed using CCSD(T)/aug-cc-pV(D+d)Z on an unrestricted Hartree-Fock reference using CFOUR[64], with the starting geometry optimized at the same level of theory in CFOUR. The IRC trajectory is included in the Supplementary Information.†

2.2 Energies

Convergence of the relative electronic energies with respect to method and basis set was monitored by the focal point approach of Allen and co-workers.[65–68] For each species, the energy was computed using correlation-consistent basis sets up to aug-cc-pV(5+D)Z[57–60] at the UCCSD(T) level. The energy

was then extrapolated to the complete basis set (CBS) limit.[69,70] This energy, relative to that of the reactants, is $\Delta E_{\mathrm{e,CBS}}$. To obtain the final energy, the following corrections, relative to water and SO, were added to $\Delta E_{\mathrm{e,CBS}}$:

1. To estimate the contribution of full triple excitations and perturbative quadruple excitations, the following correction was computed using the aug-cc-pV(D+d)Z basis set with both CCSD(T)/ROHF and CCSDT(Q)/ROHF methods in MRCC,[71] using the CCSDT(Q)/B ansatz, per previous studies[72]:

$$\Delta_{\mathrm{T(Q)}} = \Delta E_{\mathrm{CCSDT(Q)}} - \Delta E_{\mathrm{CCSD(T)}}.$$

2. To estimate the effect of the frozen core approximation, the energy was corrected with the difference between energies with and without the frozen core approximation at the UCCSD(T)/aug-cc-pWCQZ level[59,61] using MOLPRO 2010.1:[56]

$$\Delta_{\mathrm{CORE}} = \Delta E_{\mathrm{AE\text{-}CCSD(T)}} - \Delta E_{\mathrm{CCSD(T)}}.$$

3. To estimate relativistic effects, a scalar correction was computed at the all-electron CCSD(T)/aug-cc-pCVTZ level[59,61] in CFOUR 1.0. The following correction from direct perturbation theory at second order in c^{-1} (DPT2) includes the Darwin-term and one-electron and two-electron mass-velocity terms:[73,74]

$$\Delta_{\mathrm{REL}} = \Delta E_{\mathrm{AE\text{-}CCSD(T)/DPT2}} - \Delta E_{\mathrm{AE\text{-}CCSD(T)}}.$$

4. To estimate the effect of the Born–Oppenheimer approximation, the diagonal Born–Oppenheimer correction[75,76] was computed using the aug-cc-pV(T+d)Z[57–60] basis set, at the ROHF level in CFOUR.[64] In this correction, $\hat{T}_n$ is the nuclear kinetic energy operator and $\Psi_e(r;R)$ is the electronic wavefunction with parametric dependence on nuclear coordinates.

$$\Delta_{\mathrm{DBOC}} = \langle \Psi_e(r;R) | \hat{T}_n | \Psi_e(r;R) \rangle .$$

To obtain the final enthalpy at zero kelvin, relative to water and SO, the difference in harmonic zero point vibrational energy (ZPVE) between the complex and the reactants was added to the relative electronic energy. The harmonic ZPVE used was the ZPVE coming from the frequencies computed in the previous section.

Lastly, to decompose the binding energy into physically meaningful terms, the open-shell variant of SAPT0 implemented in Psi4 was used.[77–79] The use of SAPT0 allows computation of electrostatic, induction, dispersion, and exchange contributions to the binding energy. SAPT0 computations were performed on the final optimized geometries for the species studied. To compare our $SO\cdots H_2O$ complexes to $O_2\cdots H_2O$ complexes, the geometries reported by Dreux and Tschumper were used. SAPT0 computations used an unrestricted reference, the jun-cc-pV(D+d)Z basis,[80] and the jun-cc-pV(D+d)Z-ri[81] density fitting basis for density fitting within SAPT0. The jun family of basis sets are known to maximize cancellation of errors within SAPT0.[82]

3 Results and Discussion

3.1 Geometries

Optimization revealed two minimum energy $SO\cdots H_2O$ complexes at the UCCSD(T)/aug-cc-pV(Q+d)Z level of theory. The first minimum is that reported by Wakelam et al.[48] and is analogous to the single minimum found by Dreux and Tschumper[50] on the $O_2\cdots H_2O$ surface. The two structures are compared in the left column of Figure 1. In the structure of Dreux and Tschumper, one of the O_2 oxygens is hydrogen bonded to water at a distance of 2.637 Å. The hydrogen bond length in our complex is 2.123 Å. In $O_2\cdots H_2O$, the water is rotated to be closer to the other oxygen of O_2, and the distance between the oxygens of SO and H_2O is 3.297 Å compared to the 3.610 Å between the SO sulfur the H_2O oxygen. This indicates an energy-lowering oxygen-oxygen interaction in the $O_2\cdots H_2O$ structure. The O−O−H angle is nearly linear at 179.1°, but the S−O−H angle is 150.3°.

The other complex found is analogous to the $O_2\cdots H_2O$ complex labeled Complex XI by Dreux and Tschumper.[50] The two structures are compared in the right column of Figure 1. They report a C_{2v} complex with a 3.167 Å chalcogen bond between an oxygen on O_2 and the oxygen of H_2O. The complex of Dreux and Tschumper has a single b_2 imaginary mode.[50] Comparison with the results of Sabu,[49] who performed IRC computations on the structures, shows that the imaginary mode leads

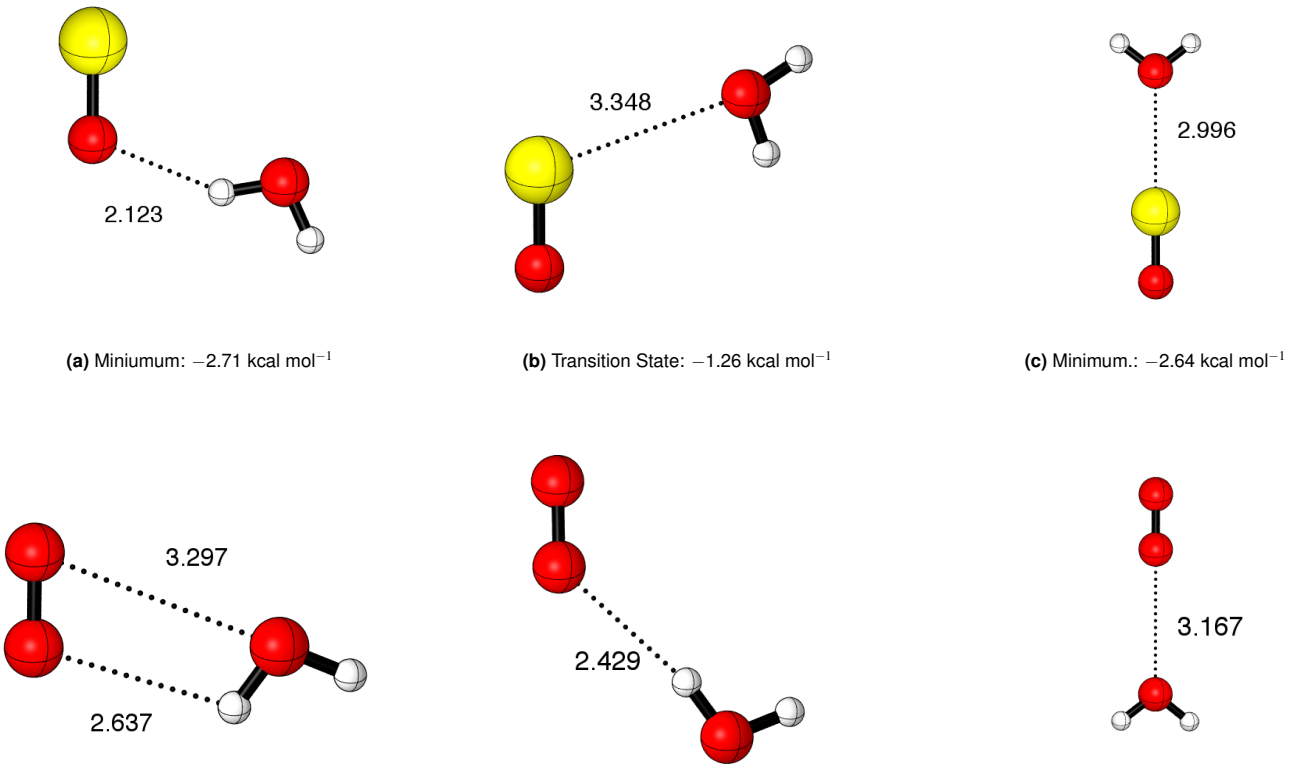

(a) Miniumum: -2.71 kcal mol^{-1} **(b)** Transition State: -1.26 kcal mol^{-1} **(c)** Minimum.: -2.64 kcal mol^{-1}

(d) Minimum: -0.70 kcal mol^{-1} **(e)** Transition State: -0.52 kcal mol^{-1} **(f)** Transition State: -0.33 kcal mol^{-1}

Fig. 1 The geometries of the SO$-$H$_2$O complex (top) compared to the analogous geometries of the O$_2-$H$_2$O system (bottom). The left structures are the hydrogen bonded minima, the right structures are the end-to-end chalcogen bonded complexes, and the middle structures are the transition states connecting them. The O$_2\cdots$H$_2$O geometries and energies were computed by Dreux and Tschumper[50] using UCCSD(T)/cc-pV(Q+d)Z with augmented functions on non-hydrogen atoms. The SO$\cdots$H$_2$O structures presented here were computed in this work and optimized at UCCSD(T)/aug-cc-pV(Q+d)Z. Energies do not include zero point vibrational energy. The orientation of O$_2$ and SO is found to be constant throughout the figures. Distances are in Å.

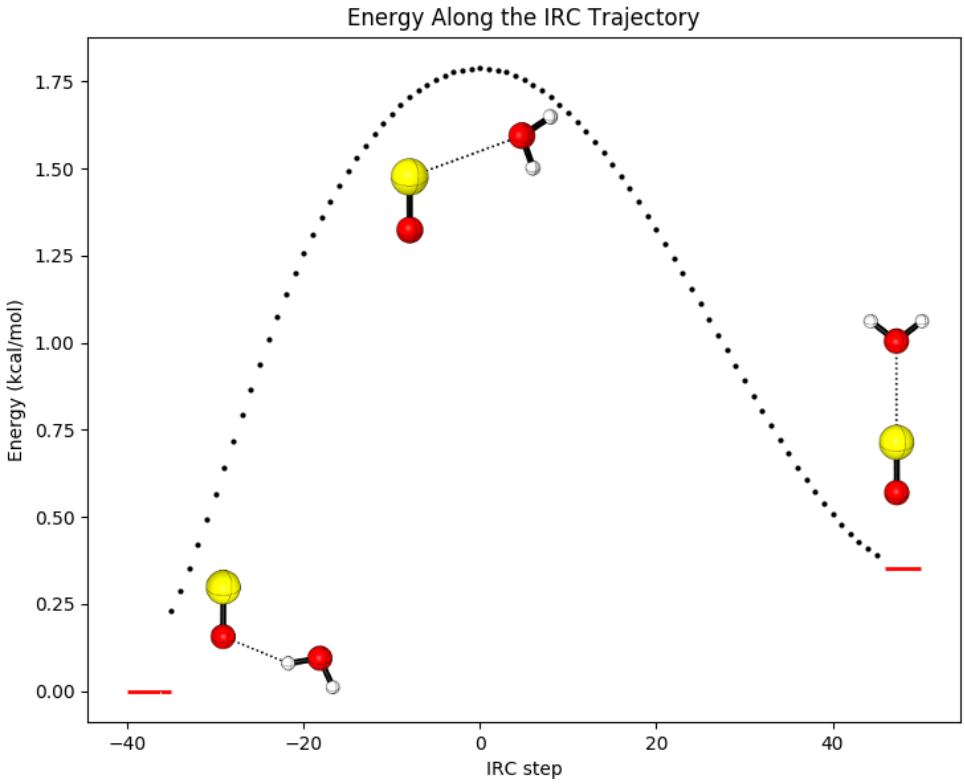

Fig. 2 The energy of $SO\cdots H_2O$ alone the intrinsic reaction coordinate (IRC) path from the hydrogen bonded structure to the chalcogen bonded structure. IRC trajectories were computed at CCSD(T)/aug-cc-pV(D+d)Z due to the flatness of the isovalent $O_2\cdots H_2O$ surface. Red lines denote energies of the optimized structures. Full IRC trajectories are available in the Supporting Information.[†]

to in-plane rotation of water to form another transition state which possesses the hydrogen bond of the energy minimum but lacks its oxygen-oxygen interaction. Our structure has a chalcogen bond between the sulfur of SO and the oxygen of H_2O at a distance of 2.996 Å. For $SO\cdots H_2O$, this structure is a minimum energy complex, not a transition state.

To investigate the possibility of other, undiscovered complexes, geometry optimizations were attempted for all $SO\cdots H_2O$ complexes analogous to those reported by Dreux and Tschumper for $O_2\cdots H_2O$, with six different functionals and both possible replacements of O_2 to SO. No other local energy minima were discovered.

The transition state and reaction path between the two complexes were also identified, and they were found to contrast starkly against $O_2\cdots H_2O$, as shown in the middle column of Figure 1. At the transition state for $SO\cdots H_2O$, the chalcogen bond between the sulfur and the oxygen of water has

extended to 3.348 Å and the water has begun to rotate in-plane. This rotation motion takes $SO\cdots H_2O$ between the two minimum energy complexes, and following the intrinsic reaction coordinate shows a smooth energy dependence, depicted in Figure 2. The transition state between the two $O_2\cdots H_2O$ complexes, however, maintains the hydrogen bond of the global minimum, but has the oxygen of water far away from O_2. To understand the path of the $O_2\cdots H_2O$ complexes, we turn to the IRCs reported by Sabu et al.[49] We infer from the connectivities reported that their head-on chalcogen bonded structure (Figure 1f) has water rotate in-plane, with minimal translation motion to move to a lower energy intermediate state (Figure 1e). The water then rotates out of plane before returning to C_s symmetry with the water oxygen now weakly chalcogen bonded to O_2 (Figure 1d). As a further difference, in $SO{-}H_2O$, the water interacts with different atoms between the two structures, but in $O_2{-}H_2O$ the dominant interaction is with the same atom in each structure.

Other stationary points discovered are reported in the Supporting Information.[†]

3.2 Energies

For all species, we observe good convergence of the energies with respect to both basis set and method. The (T) correction is no larger than 0.18 kcal mol^{-1}, and all changes observed using basis sets of at least augmented triple zeta quality are systematic. The auxiliary corrections for perturbative quadruple excitations, core correlation, relativistic effects, and breakdown of the Born–Oppenheimer approximation are all less than 0.04 kcal mol^{-1}, so no more extensive treatment is warranted. We note that as the reactants move from the hydrogen bonded geometry to the chalcogen bonded geometry, the bulk of the relative correlation energy becomes easier to recover, no longer requiring a coupled cluster treatment but only MP2. This gives the hydrogen bonded complex an electronic energy of -2.71 kcal mol^{-1} and the chalcogen bonded complex an energy of -2.64 kcal mol^{-1}.

However, upon including zero-point vibrational energy, the chalcogen bonded complex becomes the global minimum at -2.00 kcal mol^{-1}, whereas the hydrogen bonded complex has an enthalpy of -1.71 kcal mol^{-1}. The chalcogen bonded complex has a a lower zero-point vibrational energy compared to the reactants, due to having lower frequency **inter**molecular modes, shown as the last five vibrational frequencies in Table 2. For instance, the hydrogen bonded complex has its two highest intermolecular vibrational frequencies at 327 and 238 cm^{-1}, whereas the chalcogen bonded complex

Table 1 Incremented focal point table for enthalpy differences for the movement of $SO\cdots H_2O$ from the hydrogen bonded structure to the chalcogen bonded complex, relative to separated SO plus H_2O. Energies are computed as described in Section 2, using the equation: $\Delta H_{0K} = \Delta E_{e,CBS} + \Delta_{T(Q)} + \Delta_{CORE} + \Delta_{REL} + \Delta_{DBOC} + \Delta_{ZPVE}$. All energies are in kcal mol^{-1}. The geometries are shown in Figure 1

Basis Set	ΔE_e ROHF	$+\delta$ MP2	$+\delta$ UCCSD	$+\delta$ UCCSD(T)	ΔE_e Net
(A) Hydrogen Bonded Complex					
aug-cc-pV(D+d)Z	−2.38	+0.01	−0.72	−0.18	[−3.28]
aug-cc-pV(T+d)Z	−2.23	−0.03	−0.64	−0.16	[−3.06]
aug-cc-pV(Q+d)Z	−2.22	+0.08	−0.61	−0.15	[−2.90]
aug-cc-pV(5+d)Z	−2.19	+0.14	−0.62	−0.15	[−2.81]
CBS	[−2.17]	[+0.21]	[−0.62]	[−0.14]	**[–2.73]**

$$\Delta H_{0K} = -2.73 + 0.04 - 0.02 + 0.00 - 0.01 + 1.04 = \mathbf{-1.71}$$

(B) Transition State					
aug-cc-pV(D+d)Z	−0.86	−0.26	−0.27	−0.10	[−1.48]
aug-cc-pV(T+d)Z	−0.69	−0.33	−0.23	−0.11	[−1.36]
aug-cc-pV(Q+d)Z	−0.65	−0.32	−0.22	−0.11	[−1.30]
aug-cc-pV(5+d)Z	−0.63	−0.30	−0.22	−0.11	[−1.27]
CBS	[−0.62]	[−0.29]	[−0.23]	[−0.11]	**[–1.25]**

$$\Delta H_{0K} = -1.25 + 0.01 - 0.01 - 0.01 + 0.00 + 0.45 = \mathbf{-0.81}$$

(C) Chalcogen Bonded Complex					
aug-cc-pV(D+d)Z	−1.99	−0.86	+0.05	−0.16	[−2.96]
aug-cc-pV(T+d)Z	−1.62	−1.02	+0.06	−0.17	[−2.75]
aug-cc-pV(Q+d)Z	−1.57	−1.04	+0.08	−0.18	[−2.70]
aug-cc-pV(5+d)Z	−1.55	−1.00	+0.08	−0.18	[−2.65]
CBS	[−1.54]	[−0.96]	[+0.08]	[−0.18]	**[–2.60]**

$$\Delta H_{0K} = -2.60 + 0.02 - 0.03 - 0.03 + 0.00 + 0.64 = \mathbf{-2.00}$$

Table 2 Harmonic vibrational frequencies of the $SO\cdots H_2O$ structures computed at UCCSD(T)/aug-cc-pV(Q+d)Z. Changes in the five intermolecular vibrational frequencies cause the chalcogen bonded structure to have lower ΔH_{0K} than the hydrogen bonded structure, despite the hydrogen bonded structure having a higher electronic energy. All frequencies are in cm^{-1}. The geometries are shown in Figure 1. The point groups are provided and the vibrations described in the SI†

Mode Number	Hydrogen Bonded Structure	Transition State	Chalcogen Bonded Structure
ω_1	3925	3934	3937
ω_2	3809	3825	3829
ω_3	1653	1652	1651
ω_4	1153	1148	1144
ω_5	327	105	146
ω_6	238	103	98
ω_7	138	66	84
ω_8	59	58	70
ω_9	22	$49i$	61

has frequencies of 146 and 98 cm^{-1}.

We attribute this zero point energy difference between the two complexes, large enough to change which is the minimum geometry, to two effects. First, vibrations that disrupt the hydrogen bond have a smaller reduced mass and thus larger frequency, compared to vibrations that disrupt the chalcogen bond. The hydrogen bond breaking vibrations only need to move a hydrogen, whereas the chalcogen bond breaking vibrations need to move the much more massive oxygen or sulfur atoms. Second, the electrostatic component of the binding energy has a cosine dependence on the angle between the monomer dipoles. In the chalcogen bonded complex, the dipoles are perfectly aligned at 180°, but the dipoles of the monomers of the hydrogen bonded complex are not. The cosine function has greater sensitivity to perturbations in the angle away from 0 or 180 degrees, so the electrostatic energy likely increases more for comparable displacements, leading to larger harmonic vibrational frequencies for the hydrogen bonded complex.

With respect to separated $SO\cdots H_2O$, the transition state has a zero kelvin enthalpy of -0.81 kcal mol^{-1}, but it has an electronic energy of -1.26 kcal mol^{-1}, giving an electronic energy of activation of approximately 1.4 kcal mol^{-1} from each side. This is in stark contrast to the $O_2\cdots H_2O$ system, where eleven first and second order saddle points had were less than 0.5 kcal mol^{-1} above the global minimum in electronic energy.

3.3 Energy Decomposition Analysis

To interpret the differences in the presented stationary points of the potential energy surfaces, we turn to the energy decomposition analysis of SAPT0, shown in Figure 3.

All contributions to the binding energy in $O_2\cdots H_2O$ are minuscule in comparison with the binding energy contributions in $SO\cdots H_2O$. The strongest attractive interaction between O_2 and H_2O is a -0.54 kcal mol^{-1} electrostatic contribution from the hydrogen bonded complex, shown in Figure 1d. Since O_2 has no permanent dipole, any electrostatic interaction with H_2O must be through higher-order terms of the multipole expansion, resulting in a low electrostatic contribution to the binding energy. The exchange contributions for $O_2\cdots H_2O$ are consistently low, but tend to decrease moving from the hydrogen bonded structure to the structure where the two oxygens interact in a weak chalcogen bond; see Figure 1f. The two molecules get further apart along this path, and reduced overlap explains the decreasing significance of the exchange term. The small induction contribution is a consequence of both oxygen's poor polarizability[83] and molecular oxygen not having a dipole to induce a charge on water. Dispersion is weak due to $O_2\cdots H_2O$ being far apart and having few electrons, relative to $SO\cdots H_2O$. We expect that any increase in dispersion strength from the two molecules approaching would be more than compensated for by an increase in the exchange interaction.

Turning to the SAPT decomposition for $SO\cdots H_2O$, we see much larger attractive contributions, including -4.30 and -4.44 kcal mol^{-1} electrostatic contributions for the hydrogen bonded (Figure 1a) and the chalcogen bonded structures (Figure 1c), respectively. This decreases to -1.94 kcal mol^{-1} for the transition state between the two, indicating the reason for the differences between the $O_2\cdots H_2O$ and $SO\cdots H_2O$ surfaces: SO and H_2O have interactions strong enough to cause changes in energy over 1 kcal mol^{-1} when transitioning between minima.

We explain the individual contributions as follows: SO has a relatively strong dipole of 1.55 debye,[84] allowing for a strong electrostatic interaction with H_2O. Although the dipoles are perfectly aligned in the chalcogen bonded structure (Figure 1c), the monomers of the chalcogen bonded structure are more separated than in the hydrogen bonded structure (Figure 1a), causing the electrostatic contributions to be approximately equal. This proximity effect is also responsible for the magnitude of the exchange contributions. Because sulfur has an additional valence shell compared to oxygen,

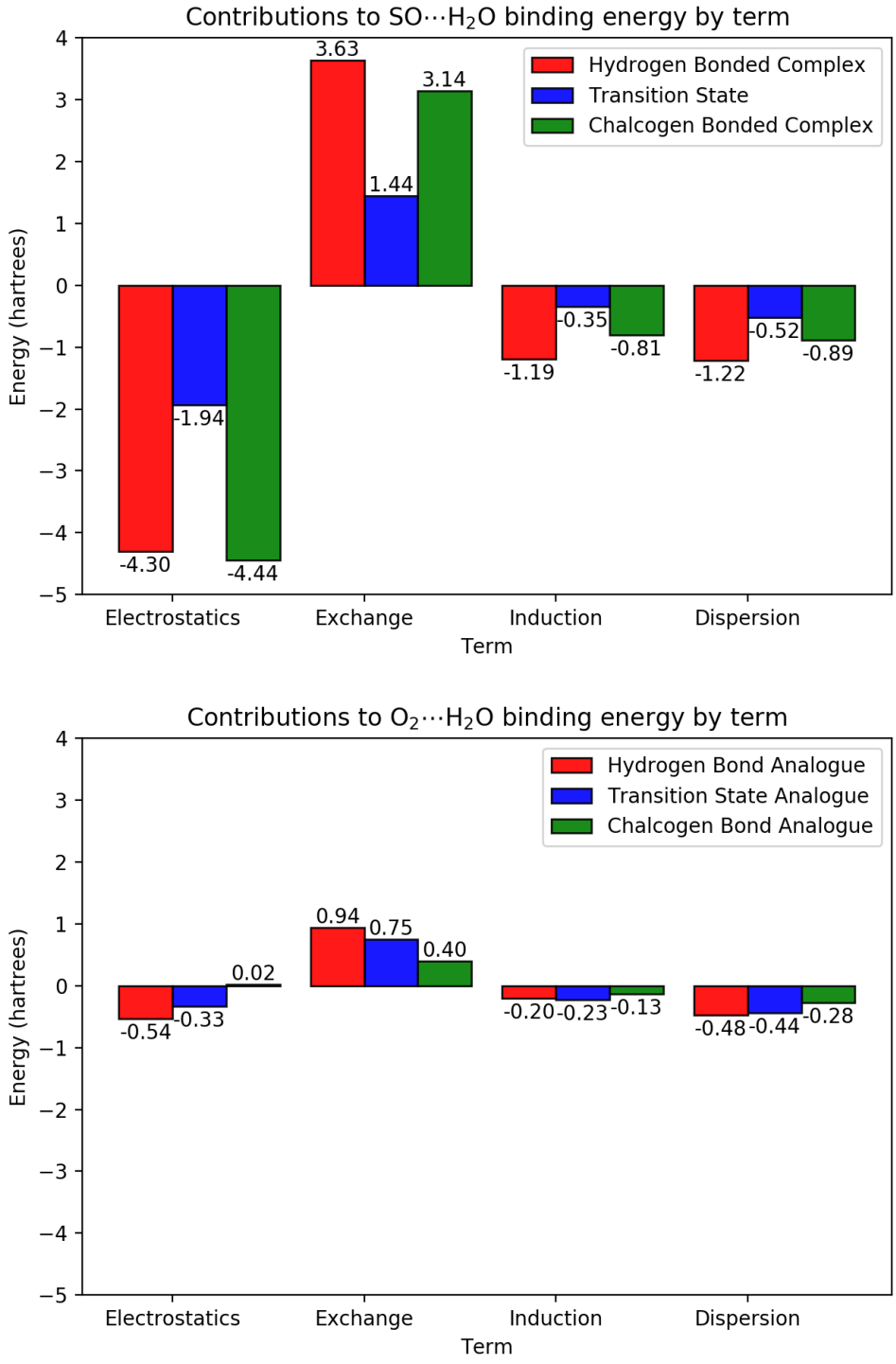

Fig. 3 The decomposition of the binding energies of $SO\cdots H_2O$ and $O_2\cdots H_2O$ according to open-shell SAPT0. Geometries are those shown in Figure 1 and reported in detail in the Supporting Information.† SAPT0 computations were performed with the jun-cc-pV(D+d)Z basis and the jun-cc-pV(D+d)Z-ri density fitting basis

we expect greater exchange overlap between SO and H_2O compared to O_2 and H_2O, explaining the difference in exchange interactions. The increase in induction magnitude is a consequence not only of the polarity of SO but its greater polarizability.[85] Lastly, the increase in dispersion is because both sulfur has more electrons to disperse than oxygen does, and the intermolecular distance for $SO\cdots H_2O$ tends to be smaller than for $O_2\cdots H_2O$. The greater distance between the two complexes in the chalcogen bonded complex leads to the reduction in magnitude of the exchange, induction, and dispersion terms.

Finally, we can use the SAPT0 decomposition results to make sense of the differences in the geometries of the two species. $SO\cdots H_2O$ has a hydrogen bonded and a chalcogen bonded complex that are approximately as favorable energetically, and the complexes smoothly rotate from one to the other. But in $O_2\cdots H_2O$, the possible hydrogen bond and the chalcogen bond are both so weak that it is advantageous to have both interactions at once. This is energetically preferred to optimizing the strength of either interaction. We note that both the hydrogen bond and the chalcogen bond induce a polarization on O_2 beneficial to the other interaction.

Whereas the complexes of $SO\cdots H_2O$ can be understood primarily through their strongest interaction, the electrostatics, the interactions in the $O_2\cdots H_2O$ complexes are weak enough that all interactions must be considered at once. The minimum (Figure 1a) has a favorable hydrogen bond, and the oxygen of water is able to form a very weak chalcogen bond with the opposite oxygen of O_2, decreasing the distance between water and oxygen and thus increasing the dispersion. There is no strong oxygen-oxygen interaction to cause the water to rotate up, like with $SO\cdots H_2O$, but it can rotate out of plane with only minimal energy gain (Figure 1b). The lost electrostatic energy is approximately balanced by the lost exchange penalty, and although the oxygen of water is turned away from O_2, the hydrogen bond length decreases, so dispersion effects barely change. However, when the water rotates again to the exclusively chalcogen bonded structure with an oxygen of O_2 (Figure 1c), the electrostatic advantage is almost completely lost, but exchange penalty decreases due to the molecules being further apart. Induction and dispersion decrease as well this time, so the energy goes up significantly.

4 Conclusions

We have studied the complexes formed between SO in its triplet ground state and H_2O. We have obtained geometries for the complexes and the connecting transition state with the UCCSD(T)/aug-cc-pV(Q+d)Z method. Neither the second complex nor the transition state connecting the complexes were reported by Wakelam et al.[48] The previously studied complex was held together by a hydrogen bond, while our new complex adheres due to a chalcogen bond between the oxygen of H_2O and the sulfur of SO. We have further obtained energies for these structures, relative to the constituent monomers, with CCSD(T)/CBS, including corrections for full triples and perturbative quadruples, the frozen core approximation, the non-relativistic approximation, and the Born–Oppenheimer approximation. The smooth convergence of the focal point table and the smallness of the corrections attest to the accuracy of the methods employed. We find that the hydrogen bonded complex has an energy of -2.71 kcal mol^{-1}, while the chalcogen bonded complex has an energy of -2.64 kcal mol^{-1}. Adding the relative zero point vibrational energy causes the relative energetic order of the two complexes to swap. The hydrogen bonded complex has a higher zero kelvin enthalpy of -1.71 kcal mol^{-1}, and the chalcogen bonded complex has the lower enthalpy of -2.00 kcal mol^{-1}. The transition state was found to have an enthalpy of -0.81 kcal mol^{-1}, showing it lies below separated SO plus H_2O.

SAPT0 was used to decompose the binding energy of the $SO\cdots H_2O$ and $O_2\cdots H_2O$ complexes, so the differences between their surfaces could be interpreted. We found that although the two complexes are isovalent, the interactions holding $O_2\cdots H_2O$ together are very weak, but $SO\cdots H_2O$ can be held together relatively strongly. This is because of SO's polarity allowing for more electrostatic interactions, its polarizability allowing for induction interactions, and its larger number of electrons allowing for dispersion interactions. This leads to $SO\cdots H_2O$ having a potential surface with noticeable changes in binding energies and smooth trajectories as the strong interactions break and form, whereas $O_2\cdots H_2O$ has a very flat potential surface and more chaotic trajectories due to a lack of strong interactions to anchor it.

Acknowledgements

We acknowledge Andrea Bootsma for helpful discussion on the interpretation of SAPT0 results. We acknowledge support from the National Science Foundation, Grant No. CHE-1661604.

Conflict of interest

There are no conflicts to declare.

References

1 J. T. Herron and R. E. Huie, *Chem. Phys. Lett.*, 1980, **76**, 322–324.

2 D. J. Meschi and R. J. Myers, *J. Am. Chem. Soc.*, 1956, **78**, 6220–6223.

3 P. W. Schenk and R. Steudel, *Angew. Chem. Int. Ed.*, 1965, **4**, 402–409.

4 L. Yao, O. Garmash, F. Bianchi, J. Zheng, C. Yan, J. Kontkanen, H. Junninen, S. B. Mazon, M. Ehn, P. Paasonen, M. Sipilä, M. Wang, X. Wang, S. Xiao, H. Chen, Y. Lu, B. Zhang, D. Wang, Q. Fu, F. Geng, L. Li, H. Wang, L. Qiao, X. Yang, J. Chen, V.-M. Kerminen, T. Petäjä, D. R. Worsnop, M. Kulmala and L. Wang, *Science*, 2018, **361**, 278–281.

5 R. Donovan and D. Little, *Chem. Phys. Lett.*, 1972, **13**, 488–490.

6 G. Black, R. Sharpless and T. Slanger, *Chem. Phys. Lett.*, 1982, **93**, 598–602.

7 K. Tsuchiya, K. Kamiya and H. Matsui, *Int. J. Chem. Kin.*, 1997, **29**, 57–66.

8 Z. Wu, B. Lu, R. Feng, J. Xu, Y. Lu, H. Wan, A. K. Eckhardt, P. R. Schreiner, C. Xie, H. Guo and X. Zeng, *Chem. Comm.*, 2018, **54**, 1690–1693.

9 I. A. Gargurevich, *Ind. Eng. Chem. Res.*, 2005, **44**, 7706–7729.

10 D. Bongartz and A. F. Ghoniem, *Combust. Flame*, 2015, **162**, 544–553.

11 P. Glarborg, D. Kubel, K. Dam-Johansen, H.-M. Chiang and J. W. Bozzelli, *Int. J. Chem. Kin.*, 1996, **28**, 773–790.

12 C. R. Zhou, K. Sendt and B. S. Haynes, *Proc. Combust. Inst.*, 2013, **34**, 625–632.

13 R. S. Grainger, A. Procopio and J. W. Steed, *Org. Lett.*, 2001, **3**, 3565–3568.

14 D. M. Lemal and P. Chao, *J. Am. Chem. Soc.*, 1973, **95**, 922–924.

15 I. A. Abu-Yousef and D. N. Harpp, *J. Org. Chem.*, 1997, **62**, 8366–8371.

16 M. Joost, M. Nava, W. J. Transue, M.-A. Martin-Drumel, M. C. McCarthy, D. Patterson and C. C. Cummins, *Proc. Natl. Acad. Sci. U.S.A.*, 2018, **115**, 5866–5871.

17 W. A. Schenk, *Angew. Chem. Int. Ed.*, 1987, **26**, 98–109.

18 K. K. Pandey, in *Prog. Inorg. Chem.*, John Wiley & Sons, Inc., 2007, pp. 445–502.

19 R. Wang, M. S. Mashuta, J. F. Richardson and M. E. Noble, *Inorg. Chem.*, 1996, **35**, 3022–3030.

20 A. Ishii, M. Murata, H. Oshida, K. Matsumoto and J. Nakayama, *Eur. J. Inorg. Chem.*, 2003, **2003**, 3716–3721.

21 W.-H. Leung, H. Zheng, J. L. C. Chim, J. Chan, W.-T. Wong and I. D. Williams, *J. Chem. Soc. Dalton Trans.*, 2000, 423–430.

22 M. Malischewski and K. Seppelt, *Angew. Chem. Int. Ed.*, 2017, **56**, 16495–16497.

23 W. A. Schenk, *Dalton Trans.*, 2011, **40**, 1209–1219.

24 W. A. Schenk, J. Leissner and C. Burschka, *Angew. Chem. Int. Ed.*, 1984, **23**, 806–807.

25 W. C. Swope, Y.-P. Lee and H. F. Schaefer, *J. Chem. Phys.*, 1979, **71**, 3761–3769.

26 J. M. F. Elks and C. M. Western, *J. Chem. Phys.*, 1999, **110**, 7699–7706.

27 C. P. Archer, J. M. F. Elks and C. M. Western, *J. Chem. Phys.*, 2000, **112**, 6293–6300.

28 E. Tiemann, *J. Phys. Chem. Ref. Data*, 1974, **3**, 259–268.

29 W. W. Clark and F. C. D. Lucia, *J. Mol. Spec.*, 1976, **60**, 332–342.

30 A. G. Hopkins and C. W. Brown, *J. Chem. Phys.*, 1975, **62**, 2511–2512.

31 V. Lattanzi, G. Cazzoli and C. Puzzarini, *Astrophys. J.*, 2015, **813**, 4.

32 J. B. Burkholder, E. R. Lovejoy, P. D. Hammer, C. J. Howard and M. Mizushima, *J. Mol. Spec.*, 1987, **124**, 379–392.

33 R. D. Shelton, A. H. Nielsen and W. H. Fletcher, *J. Chem. Phys.*, 1953, **21**, 2178–2183.

34 M. A. Martin-Drumel, F. Hindle, G. Mouret, A. Cuisset and J. Cernicharo, *Astrophys. J.*, 2015, **799**, 115.

35 C.-C. Zen, F.-T. Tang and Y.-P. Lee, *J. Chem. Phys.*, 1992, **96**, 8054–8061.

36 H. Wang, X. Tang, S. Zhou, W. Zhang and Y. Chu, *Chem. Phys. Lett.*, 2005, **407**, 78–82.

37 G. A. Blake, E. C. Sutton, C. R. Masson and T. G. Phillips, *Astrophys. J.*, 1987, **315**, 621.

38 G. Cazzoli, V. Lattanzi, S. Coriani, J. Gauss, C. Codella, A. A. Ramos, J. Cernicharo and C. Puzzarini, *Astron. Astrophys.*, 2017, **605**, A20.

39 G. B. Esplugues, B. Tercero, J. Cernicharo, J. R. Goicoechea, A. Palau, N. Marcelino and T. A. Bell, *Astron. Astrophys.*, 2013, **556**, A143.

40 A. S. Booth, C. Walsh, M. Kama, R. A. Loomis, L. T. Maud and A. Juhász, *Astron. Astrophys.*, 2018,

611, A16.

41 C. T. Russell and M. G. Kivelson, *J. Geophys. Res. Planets*, 2001, **106**, 33267–33272.

42 M. McGrath, *Icarus*, 2000, **146**, 476–493.

43 M. Y. Zolotov and B. Fegley, *Icarus*, 1998, **132**, 431–434.

44 X. Zhang, M.-C. Liang, F. Montmessin, J.-L. Bertaux, C. Parkinson and Y. L. Yung, *Nat. Geosci.*, 2010, **3**, 834–837.

45 C. Y. Na, L. W. Esposito and T. E. Skinner, *J. Geophys. Res. Atmos.*, 1990, **95**, 7485.

46 A. Montoya, K. Sendt and B. S. Haynes, *J. Phys. Chem. A*, 2005, **109**, 1057–1062.

47 A. J. Frank, M. Sadílek, J. G. Ferrier and F. Tureček, *J. Am. Chem. Soc.*, 1997, **119**, 12343–12353.

48 V. Wakelam, J.-C. Loison, R. Mereau and M. Ruaud, *Mol. Astrophys.*, 2017, **6**, 22–35.

49 A. Sabu, S. Kondo, N. Miura and K. Hashimoto, *Chem. Phys. Lett.*, 2004, **391**, 101–105.

50 K. M. Dreux and G. S. Tschumper, *Comput. Theor. Chem.*, 2015, **1072**, 21–27.

51 Y. Kasai, E. Dupuy, R. Saito, K. Hashimoto, A. Sabu, S. Kondo, Y. Sumiyoshi and Y. Endo, *Atmos. Chem. Phys.*, 2011, **11**, 8607–8612.

52 P. J. Knowles, C. Hampel and H.-J. Werner, *J. Chem. Phys.*, 1993, **99**, 5219–5227.

53 J. D. Watts, J. Gauss and R. J. Bartlett, *J. Chem. Phys.*, 1993, **98**, 8718–8733.

54 C. Hampel, K. A. Peterson and H.-J. Werner, *Chem. Phys. Lett.*, 1992, **190**, 1–12.

55 M. J. Deegan and P. J. Knowles, *Chem. Phys. Lett.*, 1994, **227**, 321–326.

56 Molpro, *version 2010.1, a package of ab initio programs written by H.-J. Werner, P. J. Knowles, G. Knizia, F. R. Manby, M. Schütz, P. Celani, T. Korona, R. Lindh, A. Mitrushenkov, G. Rauhut, K. R. Shamasundar, T. B. Adler, R. D. Amos, A. Bernhardsson, A. Berning, D. L. Cooper, M. J. O. Deegan, A. J. Dobbyn, F. Eckert, E. Goll, C. Hampel, A. Hesselmann, G. Hetzer, T. Hrenar, G. Jansen, C. Köppl, Y. Liu, A. W. Lloyd, R. A. Mata, A. J. May, S. J. McNicholas, W. Meyer, M. E. Mura, A. Nicklaß, D. P. O'Neill, P. Palmieri, D. Peng, K. Pflüger, R. M. Pitzer, M. Reiher, T. Shiozaki, H. Stoll, A. J. Stone, R. Tarroni, T. Thorsteinsson, M. Wang, and A. Wolf, see* `http://www.molpro.net`.

57 T. H. Dunning, *J. Chem. Phys.*, 1989, **90**, 1007–1023.

58 D. E. Woon and T. H. Dunning, *J. Chem. Phys.*, 1993, **98**, 1358–1371.

59 R. A. Kendall, T. H. Dunning and R. J. Harrison, *J. Chem. Phys.*, 1992, **96**, 6796–6806.

60 T. H. Dunning, K. A. Peterson and A. K. Wilson, *J. Chem. Phys.*, 2001, **114**, 9244–9253.

61 K. A. Peterson and T. H. Dunning, *J. Chem. Phys.*, 2002, **117**, 10548–10560.

62 C. Gonzalez and H. B. Schlegel, *J. Phys. Chem.*, 1990, **94**, 5523–5527.

63 R. M. Parrish, L. A. Burns, D. G. A. Smith, A. C. Simmonett, A. E. DePrince, E. G. Hohenstein, U. Bozkaya, A. Y. Sokolov, R. D. Remigio, R. M. Richard, J. F. Gonthier, A. M. James, H. R. McAlexander, A. Kumar, M. Saitow, X. Wang, B. P. Pritchard, P. Verma, H. F. Schaefer, K. Patkowski, R. A. King, E. F. Valeev, F. A. Evangelista, J. M. Turney, T. D. Crawford and C. D. Sherrill, *J. Chem. Theory Comput.*, 2017, **13**, 3185–3197.

64 J. F. Stanton, J. Gauss, L. Cheng, M. E. Harding, D. A. Matthews and P. G. Szalay, *CFOUR, Coupled-Cluster techniques for Computational Chemistry, a quantum-chemical program package*, With contributions from A.A. Auer, R.J. Bartlett, U. Benedikt, C. Berger, D.E. Bernholdt, Y.J. Bomble, O. Christiansen, F. Engel, R. Faber, M. Heckert, O. Heun, M. Hilgenberg, C. Huber, T.-C. Jagau, D. Jonsson, J. Jusélius, T. Kirsch, K. Klein, W.J. Lauderdale, F. Lipparini, T. Metzroth, L.A. Mück, D.P. O'Neill, D.R. Price, E. Prochnow, C. Puzzarini, K. Ruud, F. Schiffmann, W. Schwalbach, C. Simmons, S. Stopkowicz, A. Tajti, J. Vázquez, F. Wang, J.D. Watts and the integral packages MOLECULE (J. Almlöf and P.R. Taylor), PROPS (P.R. Taylor), ABACUS (T. Helgaker, H.J. Aa. Jensen, P. Jørgensen, and J. Olsen), and ECP routines by A. V. Mitin and C. van Wüllen. For the current version, see http://www.cfour.de.

65 M. S. Schuurman, S. R. Muir, W. D. Allen and H. F. Schaefer, *J. Chem. Phys.*, 2004, **120**, 11586–11599.

66 J. M. Gonzales, C. Pak, R. S. Cox, W. D. Allen, H. F. Schaefer, A. G. Császár and G. Tarczay, *Chem. Eur. J.*, 2003, **9**, 2173–2192.

67 A. G. Császár, W. D. Allen and H. F. Schaefer, *J. Chem. Phys.*, 1998, **108**, 9751–9764.

68 A. L. L. East and W. D. Allen, *J. Chem. Phys.*, 1993, **99**, 4638–4650.

69 D. Feller, K. A. Peterson and T. D. Crawford, *J. Chem. Phys.*, 2006, **124**, 054107.

70 T. Helgaker, W. Klopper, H. Koch and J. Noga, *J. Chem. Phys.*, 1997, **106**, 9639–9646.

71 M. Kállay, Z. Rolik, J. Csontos, I. Ladjánszki, L. Szegedy, B. Ladóczki, G. Samu, K. Petrov, M. Farkas, P. Nagy *et al.*, *See also: http://www.mrcc.hu*, 2015.

72 J. M. Martin, *Mol. Phys.*, 2013, **112**, 785–793.

73 W. Klopper, *J. Comp. Chem.*, 1997, **18**, 20–27.

74 G. Tarczay, A. G. Császár, W. Klopper and H. M. Quiney, *Mol. Phys.*, 2001, **99**, 1769–1794.

75 N. C. Handy, Y. Yamaguchi and H. F. Schaefer, *J. Chem. Phys.*, 1986, **84**, 4481–4484.

76 H. Sellers and P. Pulay, *Chem. Phys. Lett.*, 1984, **103**, 463–465.

77 E. G. Hohenstein and C. D. Sherrill, *J. Chem. Phys.*, 2010, **132**, 184111.

78 E. G. Hohenstein, R. M. Parrish, C. D. Sherrill, J. M. Turney and H. F. Schaefer, *J. Chem. Phys.*, 2011, **135**, 174107.

79 J. F. Gonthier and C. D. Sherrill, *J. Chem. Phys.*, 2016, **145**, 134106.

80 E. Papajak and D. G. Truhlar, *J. Chem. Theory Comput.*, 2011, **7**, 10–18.

81 F. Weigend, A. Köhn and C. Hättig, *J. Chem. Phys.*, 2002, **116**, 3175–3183.

82 T. M. Parker, L. A. Burns, R. M. Parrish, A. G. Ryno and C. D. Sherrill, *J. Chem. Phys.*, 2014, **140**, 094106.

83 T. N. Olney, N. Cann, G. Cooper and C. Brion, *Chem. Phys.*, 1997, **223**, 59–98.

84 F. X. Powell and D. R. Lide, *J. Chem. Phys.*, 1964, **41**, 1413–1419.

85 V. Aquilanti, D. Ascenzi, E. Braca, D. Cappelletti, G. Liuti, E. Luzzatti and F. Pirani, *J. Phys. Chem. A*, 1997, **101**, 6523–6527.